

# Emergency Control Strategy for Power Systems with Renewables Considering a Utility-scale Energy Storage Transient

Xuekuan Xie, *Student Member, IEEE*, Yuchen Zhang<sup>✉</sup>, *Member, IEEE*, Ke Meng, *Member, IEEE*, Zhao Yang Dong, *Fellow, IEEE*, and Junwei Liu, *Member, IEEE*

**Abstract**—Integration of renewable energy generators has greatly altered both static and dynamic characteristics of the system. Combined with the uncertainties it introduced, the risk of a system being transient instable is significantly alleviated. This paper proposes a multi-objective coordinated post-contingency control method. It aims to increase post-contingency system security with emergence control (EC) while minimizing the total control cost. Two ECs are adopted in this paper: energy storage systems (ESSs) and emergency load shedding (ELS). ESSs are immediately connected to the network after contingency occurrence to provide both active and reactive power support. ELS will be triggered when the support from ESSs is insufficient to stabilize the system to prevent further deterioration of system security. Performance of the proposed method was evaluated on a modified New England 39-bus benchmark system. The results indicate that the proposed method can find solutions to stabilize the system against credible contingencies and optimally balance between system stability and economy.

**Index Terms**—Emergency control, energy storage, renewable energy uncertainty, system modelling, transient stability.

## I. INTRODUCTION

**B**EING an efficient method to alleviate energy shortage problems and reduce pollution, renewable energy sources, especially wind power, are playing an increasingly important role in supporting system power balance. However, the integration of large-scale wind farms shows serious impacts to the transmission systems, resulting from its intermittent and stochastic nature [1]. Furthermore, the increased percentage of asynchronous generators, e.g. wind generators, will reduce system inertia. It will lead to more dramatic system dynamic performances, thus deteriorating the system security level and harming system transient stability.

Large-disturbance rotor angle stability, also referred to as transient stability, measures the ability of a power system to

maintain synchronism subject to a significant disturbance [2]. It is the most stringent criterion as loss will likely result in catastrophic consequences, including cascading failures and system shutdowns. Depending on the time of actuation, control methods to maintain stable system operation are classified into two categories, preventive control (PC) and corrective control (CC). A blackout event occurred in South Australia in Sept. 2016 [3] inferred the importance to have a timely CC method to assist PC, especially for systems with high penetration of wind power under multi-contingency conditions.

The existing CC methods are response-driven (e.g. UVLS and UFLS), which act as the final resort for system stabilization [4]. They depend on the long-term response of the system and cannot respond in time to prevent the propagation of instability. The event-driven CC methods, also referred to as Emergency Control (EC), aims to provide in-time system performance improvement by executing immediately after contingencies. Among the common EC methods, Emergency Load Shedding (ELS) immediately cuts off a certain amount of load after contingencies, which has been identified and widely adopted as an effective and fast method to stabilize the system [4].

Recent years have seen the increased deployment of energy storage systems (ESSs), especially in utility-scale, to provide extra flexibility in systems operating against uncertainties and targeted to enhance system transient stability [5], [6]. To achieve this goal, various studies were performed. A study was performed in [7] to illustrate the effectiveness of enhancing system transient stability by the placing of battery energy storage systems (BESSs). It also evaluated the impact of DC-side contingencies of BESSs on the AC network [8] presented a methodology to enhance system transient stability via applying a central area controller on a wind turbine with a battery storage connection. Apart from a battery, other forms of energy storage were also considered, such as a model predictive control-based controlling strategy in [9], which utilized superconducting magnetic energy storage (SMES); and the application of supercapacitor energy storage systems in microgrids were presented in [10]. However, uncertainties were rarely considered apart from our previous paper [11], and some ESS models were over-simplified and unable to replicate their dynamic performances. Moreover, a generalized ESS model was proposed in [12], based on the voltage

Manuscript received September 28, 2019; revised May 3, 2020; accepted July 20, 2020. Date of online publication August 19, 2020; date of current version February 28, 2021. This work was supported by Arc Research Hub for Integrated Energy Storage Solutions (IH180100020).

X. K. Xie, Y. C. Zhang (corresponding author, e-mail: yuchen.zhang6@unsw.edu.au; ORCID: <https://orcid.org/0000-0002-1211-2427>), K. Meng, Z. Y. Dong and J. W. Liu are with the School of Electrical Engineering and Telecommunications, University of New South Wales, Sydney, NSW 2052.

DOI: 10.17775/CSEEJPES.2019.02320

source converter (VSC), to capture a more accurate dynamic performance for transient and voltage stability analysis.

This paper presents a multi-objective coordinated emergency control method, which optimizes the cost generated from two EC actions, i.e. ESS transient control and ELS, while maintaining system stability. The ESSs will provide continuous active/reactive power control to the post-contingency system, and ELS will be activated if ESSs are insufficient or unavailable to stabilize the system. Global indicators based on the overall system performance under representative scenarios are also developed in this paper to evaluate system stability and EC costs. Strategy tables targeting credible contingencies were also generated for system operators.

The paper is organized as follows: Section II introduces the mathematical formulation of the proposed method; Section III presents the solution methodologies, which includes a brief analogy on the dynamic battery model; Section IV presents the numerical outcomes of the simulation performed on benchmark system and Section V presents the discussions and conclusions.

## II. MATHEMATICAL MODEL

The method proposed involves a multi-objective optimization problem, which aims to trade-off between two objectives under various equality and inequality constraints. The mathematical model is introduced in this section.

### A. Multi-objective Optimization

The multi-objective optimization model proposed in this paper consists of two parts: main objective function and constraints. The main objective function includes two objectives, which focus on maximizing system performance (quantified by system performance indicators) and minimizing economic impact (operational cost) respectively. The constraints include static and dynamic. The static constraints clarify the pre-contingency operational requirements under static load flow, such as the supply-demand balance and operational limits. The dynamic constraints emphasize the post-contingency system operational requirements, such as the power balance to be maintained in the presence of post-contingency controls and the minimum level of system performance standards under such conditions.

The mathematical representations of the model are shown in (1)–(5):

$$\min_{\mathbf{u}} F[f_1(\mathbf{x}, \mathbf{u}, \mathbf{v}), f_2(\mathbf{x}, \mathbf{u}, \mathbf{v})] \quad (1)$$

$$\text{s.t } \mathbf{g}^0(\mathbf{y}^0, \mathbf{u}, \mathbf{w}^{\text{UC}}) = \mathbf{L}^0 \quad (2)$$

$$\mathbf{h}_S^0(\mathbf{x}^0, \mathbf{y}^0, \mathbf{u}, \mathbf{w}^{\text{UC}}) \leq 0 \quad (3)$$

$$\mathbf{g}(\mathbf{y}, \mathbf{u}, \mathbf{w}^{\text{UC}}) = \mathbf{L}^0 - \mathbf{L}^{\text{ELS}} \quad (4)$$

$$\mathbf{h}_D(\mathbf{x}, \mathbf{y}, \mathbf{u}, \tilde{\mathbf{w}}) \leq 0 \quad (5)$$

where the main objective function is denoted by  $F$ , with  $f_1$  and  $f_2$  representing its objectives, namely expected transient stability index (ETSI), and expected post-contingency control cost.  $\mathbf{g}$  and  $\mathbf{h}$  are the notation for equality and inequality constraints, with superscript “0” representing the initial condition.  $\mathbf{x}$  is the system state variable array, which consists

of variables, such as generator angles and rotor speed.  $\mathbf{y}$  is the system changing variable array, for example bus voltage magnitudes and phase angle with respect to the slack bus.  $\mathbf{u}$ ,  $\mathbf{v}$  and  $\mathbf{w}^{\text{UC}}$  represent control variables, state variables and uncertainty variables respectively.  $\mathbf{L}^0 = [L_1^0, \dots, L_i^0, \dots, L_n^0]$  is the initial load demand on each of the buses in the test system, and  $\mathbf{L}^{\text{ELS}} = [L_1^{\text{ELS}}, \dots, L_i^{\text{ELS}}, \dots, L_n^{\text{ELS}}]$  is the amount of load reduction under ELS on each bus. Control variable vector  $\mathbf{u}$  is represented as follows:

$$\mathbf{u} = [\beta_1, \beta_2, \dots, \beta_i] \quad (6)$$

in which  $\beta_i$  represents the percentage of load reduction on the  $i$ -th bus under ELS.

### B. Objective 1: Expected Transient Stability Index

The index adopted to measure system transient stability in this paper is stability margin  $\eta$ , calculated by extended equal-area criteria (EEAC) [13]. The EEAC method, also known as the single-machine Equivalent (SIME) method, classifies the machines in the testing system into two clusters, namely critical machines (CMs) and non-critical machines (NMs), based on their rotor angle trajectories. Each of the two clusters will be converted to its equivalent machine, and the multi-machine testing system is thus converted into its two-machine equivalent model. After further simplifying the equivalent two-machine system model into the one-machine infinite bus (OMIB) system, the system stability margin can be obtained by applying conventional EAC to the equivalent machine in the final OMIB system. In this way, a transient stability index (TSI) is generated to quantify system stability and replace the deterministic conclusions (either stable or unstable), and can be mathematically represented via:

$$\eta = A_{\text{dec}} - A_{\text{acc}} \quad (7)$$

where  $A_{\text{dec}}$  and  $A_{\text{acc}}$  are the decelerating and accelerating area in the conventional EAC and measure the system transient energies in the context of power system studies. Detailed explanations and deductions can be found in [13].

According to its definition, system stability margin ranges from  $-100$  to  $100$ , with  $[-100, 0)$ ,  $0$  and  $(0, 100]$  representing unstable, critical stable and stable system conditions. Larger  $\eta$  values in comparison indicate that the system is either more stable or less unstable.

To consider the performance of the system under all credible scenarios, the expected TSI (ETSI) is selected to be the overall index for system transient stability, which is calculated via:

$$E_{\text{TSI}} = - \sum_{i=1}^{N_c} \sum_{j=1}^{N_s} \varepsilon_s \eta_{sc} \quad (8)$$

where  $\varepsilon_s$  measures the probability of the  $s$ -th scenario, which will be explained with the scenario generation method in Section III-A.  $\eta_{sc}$  represents the value of TSI for contingency  $c$  under scenario  $s$ .  $N_c$  and  $N_s$  denote the total number of contingencies and scenarios respectively.

### C. Objective 2: Post-contingency Control Cost

The cost of post-contingency control includes two parts: the cost of ELS and the operational cost of energy storage systems, which can be calculated as:

$$E_{\text{cost}} = \sum_{s=1}^{N_s} \varepsilon_s \sum_{i=1}^{N_B} \int_0^{\beta_{si} L_i} \alpha_i(L) dL + \text{Cost}_{\text{ESS}} \quad (9)$$

where  $\alpha_i$  indicates the cost function of ELS on the  $i$ -th bus, which is an approximated representation of actual system operating cost and thus may not be linear. The importance of loads on different buses are also implicitly considered in the selection of  $\alpha_i$ , where a load with a higher importance level will incur more significant ELS costs compared to shedding the same amount of load on low-importance buses.  $\beta_{si}$  is the percentage of ELS on bus  $i$  under scenario  $s$ .  $L_i$  is the load demand on bus  $i$  prior to reduction, and  $N_B$  is the total number of buses in the network. In practice, due to its tremendous impact to the customers, the cost of the operating ELS will be relatively high compared to the cost of operating ESS, which makes the latter negligible. This simplifies the operational cost of EC into:

$$E_{\text{cost}} \approx \sum_{s=1}^{N_s} \varepsilon_s \sum_{i=1}^{N_B} \int_0^{\beta_{si} L_i} \alpha_i(L) dL \quad (10)$$

### D. Static Constraints

The system static constraints shown in (2) and (4) require the balance between supply and demand on each bus, shown as follows:

$$\begin{cases} P_{\text{busi}}^0 - P_{\text{busi}}^{\text{ELS}} = P_{gi} + P_{wi}^{\text{UC}} + \\ P_{\text{ESS}}^i - V_i \sum_{j=1}^{N_B} V_j (G_{ij} \cos \delta_{ij} + B_{ij} \sin \delta_{ij}) \\ Q_{\text{busi}}^0 - Q_{\text{busi}}^{\text{ELS}} = Q_{gi} + Q_{wi}^{\text{UC}} + \\ Q_{\text{ESS}}^i - V_i \sum_{j=1}^{N_B} V_j (G_{ij} \sin \delta_{ij} - B_{ij} \cos \delta_{ij}) \end{cases} \quad (11)$$

where  $P_{\text{busi}}$  and  $Q_{\text{busi}}$  are the active and reactive load on the  $i$ -th bus prior to reduction, and  $L_{\text{busi}}^0 = P_{\text{busi}} + jQ_{\text{busi}}^0$ .  $P_{\text{busi}}^{\text{ELS}}$  and  $Q_{\text{busi}}^{\text{ELS}}$  are the active and reactive load reduction on bus  $i$  under ELS, and  $L_{\text{busi}}^{\text{ELS}} = P_{\text{busi}}^{\text{ELS}} + jQ_{\text{busi}}^{\text{ELS}}$ .  $P_{gi}$  and  $Q_{gi}$  are the real and reactive power of the synchronous generator connected to the  $i$ -th bus.  $P_{wi}^{\text{UC}}$  and  $Q_{wi}^{\text{UC}}$  are the uncertain power generated by the wind farm connected to bus  $i$ .  $V_i$  and  $V_j$  represent voltage on the  $i$ -th and  $j$ -th bus respectively.  $G_{ij}$ ,  $B_{ij}$  and  $\delta_{ij}$  are the conductance, susceptance and angle difference between bus  $i$  and  $j$  respectively.

As show in (3), the operating limits under a static condition for the  $i$ -th bus focus on four aspects: real and reactive power, voltage and apparent power, shown as follows:

$$\begin{cases} |P_{gi} + P_{wi}^{\text{UC}} + P_{\text{ESS}}^i| - |P_{gi}^{\text{max}}| \leq 0, & |V_i| - |V_i^{\text{max}}| \leq 0 \\ |Q_{gi} + Q_{wi}^{\text{UC}} + Q_{\text{ESS}}^i| - |Q_{gi}^{\text{max}}| \leq 0, & |S_i| - |S_i^{\text{max}}| \leq 0 \end{cases} \quad (12)$$

where  $S_i$  is the apparent power on  $i$ -th bus and  $i \in [1, 2 \dots N_B]$ .

The active and reactive power operating constraints of ESSs are shown as follows:

$$\begin{cases} P_{\text{ESS}}^i < 0, & \text{when } \zeta^i > \zeta_{\text{max}}^i \\ P_{\text{ESS}}^i > 0, & \text{when } \zeta^i < \zeta_{\text{min}}^i \\ |P_{\text{ESS}}^i| < P_{\text{ESS}}^{i,\text{max}}, & \text{otherwise} \end{cases} \quad (13)$$

$$|Q_{\text{ESS}}^i| < Q_{\text{ESS}}^{i,\text{max}} \quad (14)$$

where  $\zeta_{\text{max}}^i$  and  $\zeta_{\text{min}}^i$  are the maximum and minimum allowable state-of-charge (SOC) of the ESS on the  $i$ -th bus.  $P_{\text{ESS}}^{i,\text{max}}$  and  $Q_{\text{ESS}}^{i,\text{max}}$  are the active and reactive capability of the ESS on the  $i$ -th bus.

### E. Dynamic Constraints

Equation (5) describes the constraints imposed during the evaluation of system dynamic behavior on the post-contingency transient stability, marked by subscript "P", and is formulated in this model as:

$$H_{sc}^{\text{TSI}}(\mathbf{x}_p, \mathbf{y}_p, \mathbf{u}, \mathbf{w}^{\text{UC}}) = \eta_{sc}, \eta_{sc} \geq 0 \quad (15)$$

where  $\eta_{sc}$  is the TSI value under scenario  $s$  and contingency  $c$ , calculated by (7), which considers system transient energies via EEAC/SIME method. The dynamic constraint requires that for any solution, it will only be acceptable if the system is stabilized under all uncertainty scenarios. In other words, any solutions resulting in negative TSI values under any scenarios will be excluded from further evaluation.

## III. SOLUTION METHODOLOGY

### A. Scenario Selection

Assuming the uncertain variable vector of a testing system is  $[\mathbf{w}^{\text{UC}}, \mathbf{S}^{\text{UC}}] = [w_1^{\text{UC}} \dots w_k^{\text{UC}}, S_1^{\text{UC}} \dots S_h^{\text{UC}}]$  with a dimension of  $k+h$ , having  $l$  testing levels each will exhaustively involve  $(k+h)^l$  combinations. While extensive research has been made on sampling techniques, such as the stochastic sampling method in [14], to reduce testing scenarios and minimizing the impact on accuracy, it is still not sufficient to relieve the calculation burden. For the purpose of further reducing test intensity, the taguchi orthogonal array testing (TOAT) method is adopted to generate representative testing scenarios with optimal coverage and accuracy. The adoption of orthogonal arrays (OAs) can dramatically reduce the number of testing scenarios from exhaustive  $(k+h)^l$  to  $N_s = (k+h)^l - (k+h)+1$ , denoted as  $L_{N_s}[(k+h)^l]$ . As a pre-requisite of TOAT to ensure its optimal coverage of scenarios, equal probability is applied for each scenario, i.e.  $\varepsilon_s = 1/N_s$ . Detailed explanation and examples are provided in [15] and [16].

### B. Pareto Optimality and Natural Aggregation Algorithm

The problem formulated in Section II is a multi-objective programming (MOP) problem, which outputs solutions that tradeoff between objectives. The set of trade-off solutions is named the Pareto Set PS and denoted by  $\mathbf{x}$ . For any tradeoff solution in the PS ( $x^* \in \mathbf{x}$ ), it will satisfy two conditions: 1)  $F(x^*) \leq F(x)$  and 2)  $F(x^*) < F(x)$  for at least one objective. In other words, no improvement can be done on an objective without impairing the other objectives.  $F(x^*) =$

$[f_1(x^*), \dots, f_n(x^*)]$  represents the Pareto Optimal Objective Vector and the set that contains all the  $F(x^*)$  vectors is named Pareto Frontier (PF) [17].

The high-dimension and non-linearity nature of MOP problems usually requires the employment of heuristic methods, such as multi-objective evolutionary algorithms (MOEAs), to find its tradeoff solutions. Recently, a new form of EA, named the natural aggregation algorithm (NAA), is proposed by our colleague in [18], which adopts a stochastic migration model to mimic the decision-making process of group-living insects, e.g., cockroaches. The individuals look for shelters, i.e., optimal solutions, when placed in the feasible region. The process of NAA involves four stages: 1) *initialization*: the population and shelters are initialized; 2) *stochastic migration*: the probability of an individual of either entering or leaving a shelter is calculated; 3) *search and crossover*: shelter mutations are made in the form of searching and new candidates are generated; and 4) *individual move and shelter update*: individuals decide their next location and update the shelters based on the outcome of mutations, which will be assessed and quantified by a fitness function.

In this paper, a weight-dependent method was adopted to find the compromise solution in the Pareto Frontier [19]. Assume the algorithm involves  $N$  objectives and generates  $M$  pareto solutions, the satisfactory degree ( $\psi_m^n$ ) of the  $n$ -th objective in the  $m$ -th Pareto Solution ( $f_m^n$ ) is first calculated via:

$$\psi_m^n = \frac{f_{m-\max}^n - f_m^n}{f_{m-\max}^n - f_{m-\min}^n} \quad (16)$$

where  $f_{m-\max}^n$  and  $f_{m-\min}^n$  are the maximum and minimum objective values found in the Pareto Solutions. The overall satisfactory degree of the  $m$ -th Pareto Solution can then be found via:

$$\psi_m = \frac{\sum_{n=1}^N \omega_n \psi_m^n}{\sum_{m=1}^M \sum_{n=1}^N \omega_n \psi_m^n} \quad (17)$$

where  $\omega_n$  is the weight factor, representing the importance of the  $n$ -th objective. Its value can be selected by end-users based on practical situations.

### C. Computing Flowchart

The computing flowchart used for the proposed method is shown in Fig. 1.

After initialization, uncertain variables, which include the SOC of ESSs and power generation of wind generators, are determined via the TOAT library. The performance of the system is then assessed against a set of credible contingencies based on historical data. With ESSs immediately considered as a form of EC, the transient stability index (TSI), i.e., swing margin  $\eta$ , of the system for each scenario, is calculated based on the EEAC/SIME method. If the system is unstable (TSI < 0), ELS will be performed to regain system stability. Operating costs and TSI values will be recorded, and the algorithm will enter the next scenario if the terminating conditions are not satisfied.

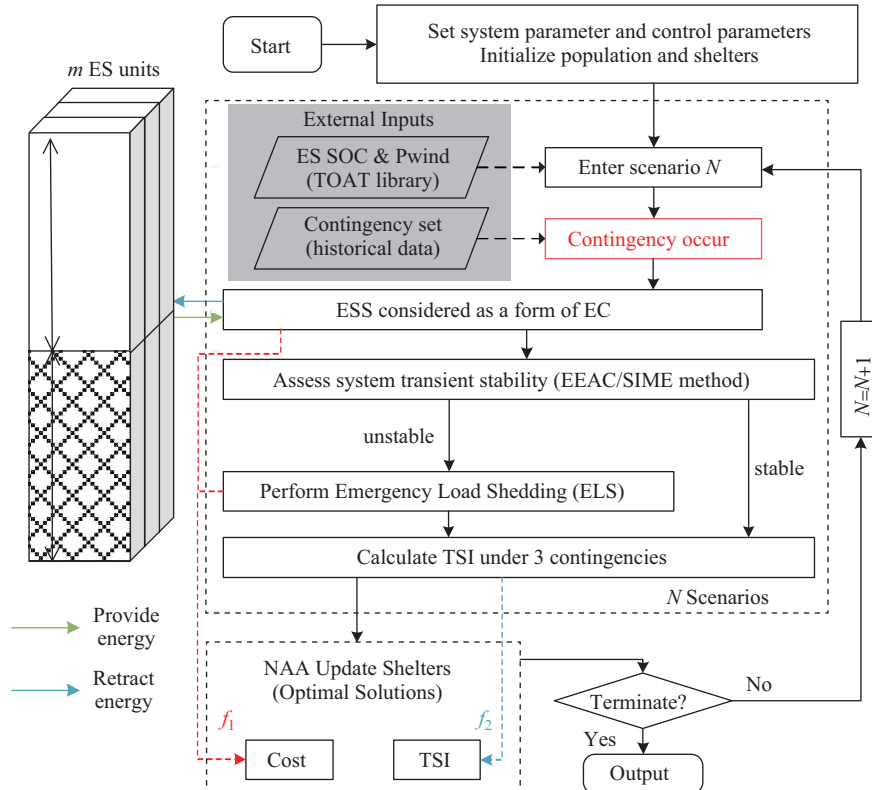


Fig. 1. Computing flowchart.

#### IV. CASE STUDY

##### A. Simulation Environment and Test System

The proposed method is tested on the New England 10-machine 39-bus system, which is a benchmark system for transient stability analysis. To consider the post-contingency dynamics of inverter-based generators, synchronous generators on bus 30 and 33 are replaced by wind farms. Two industrial-grade energy storage systems are connected to bus 8 and 24. Both changes are illustrated in Fig. 2. The 39 buses are divided into five ELS operating regions: 1) Bus 3, 25, 39 and 18; 2) Bus 26, 27, 28 and 29; 3) Bus 16, 21, 23 and 24; 4) Bus 12, 15 and 20; 5) Bus 4, 7, 8 and 31. Time-domain simulations (TDS) are performed by PSS/E, a commercial software developed by Siemens [20]. The calculation of TSI with the EEAC method is performed in MATLAB based on the results of TDS.

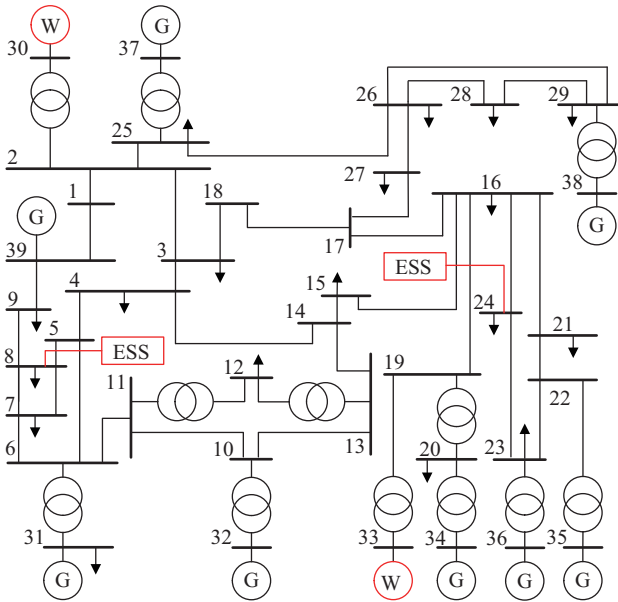


Fig. 2. Modified IEEE 10-machine 39-bus system.

To accurately model the dynamic behavior of machines and the entire network, industrial-grade models are adopted [20], [21]. Detailly, synchronous generators are modeled by GENROU with an IEEE Type-1 exciter; wind farms are modeled by a generic Type-4 wind generator and electric control models (WT4G2 and WT4E2); and ESSs are modeled by an industrial-grade battery energy storage system (BESS) model, which includes 3 modules and will be introduced in the following section.

##### B. Industrial-grade BESS Model

To achieve a better representation of the ESS under a dynamic condition compared with [11], a generic dynamic BESS model is adopted in this paper, which is developed by the Electric Power Research Institute (EPRI) [21], [22]. It includes three modules: energy generator/converter model, electrical controls model and plant control model. The block diagram illustration of the interconnected relationships between the three modules are given in Fig. 3, with details thoroughly documented in [21].

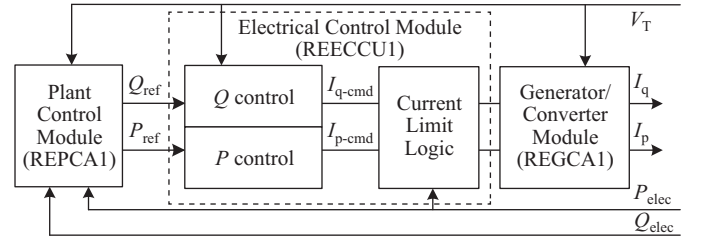


Fig. 3. Three-module Generic BESS Model.

The plant control module measures the active and reactive generation of ESS ( $P_{elec}$  and  $Q_{elec}$ ) and device terminal voltage ( $V_T$ ). The module then calculates and outputs both the active and reactive power setpoint ( $P_{ref}$  and  $Q_{ref}$ ) for the control module. The plant control module is optional, and its necessity is dependent on the operating mode of the control module.

The electrical control module models the control system of an ESS inverter. The two key inputs are the active and reactive power reference values ( $P_{ref}$  and  $Q_{ref}$ ), which are either initialized as constants or fed in from the outputs of the plant control module. Three other switching variables are available, which determines the control blocks activated and thus determining the control modes. The effects of control are output in the form of active and reactive current command values ( $I_{p-cmd}$  and  $I_{q-cmd}$ ). Additionally, it also includes a simplified representation of the charging/discharging mechanism, which is also considered in the limit logic of output command current values, as shown in Fig. 4.

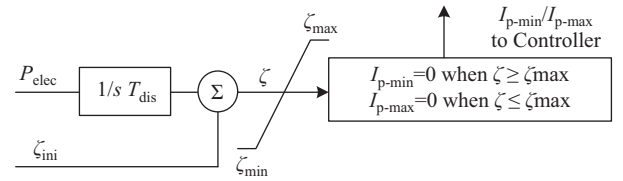


Fig. 4. BESS charging mechanism.

In Fig. 4,  $T_{dis}$  represents the charge/discharge rate of ESS,  $\zeta$  denotes the current state of charge (SOC), with  $\zeta_{min}$  and  $\zeta_{max}$  defining the allowable depth of discharge and charge. This simplified model indicates that the active current output of ESS will be limited when either  $\zeta_{min}$  or  $\zeta_{max}$  is reached, thereby limiting the real power output or input of the ESS, which is consistent with actual practice.

The generator/converter module represents the inverter interface of the ESS. The active and reactive current command ( $I_{p-cmd}$  and  $I_{q-cmd}$ ) are input from the control module. After passing reactive current management blocks, active and reactive terminal current ( $I_p$  and  $I_q$ ) are output into the network.

##### C. Base Case Scenario

The base dispatch of the system is shown in Table I, in which the asterisk marks wind farms with DFIG turbines. Three  $N - 1$  contingencies are considered, shown in Table II.

The stability margins under base dispatch against the credible contingencies are listed in Table III, with negative TSI value indicating an unstable post-contingency system.

TABLE I  
BASE DISPATCH OF NE SYSTEM

Generator	Output (MW)	Generator	Output (MW)
Gen30*	150.00	Gen35	644.93
Gen31	560.91	GEN36	552.98
Gen32	150.00	Gen37	540.00
Gen33*	624.00	Gen38	822.41
Gen34	504.13	Gen39	1000.00

TABLE II  
CONTINGENCY SET

Contingency name	Location	Duration	Line tripped
C1	Bus 4	0.28 sec	Line 4–5
C2	Bus 21	0.13 sec	Line 21–22
C3	Bus 29	0.07 sec	Line 29–26

TABLE III  
STABILITY MARGIN UNDER BASE CASE SCENARIO (WITHOUT UNCERTAINTY AND EC)

Contingency	C1	C2	C3
TSI ( $\eta$ )	-2.65	-1.82	-0.22

#### D. Multi-contingency Testing

In the simulation, uncertainties from two types of devices are considered: wind power generation and initial SOC ( $\zeta_{ini}$ ) of ESSs. For two wind generators on bus 30 and 33 introduced previously, their mean power generation ( $\mu$ ) is 150 MW, and the maximum deviation ( $\sigma$ ) is 10%. Therefore, three testing levels will be selected for interval optimization [23]:  $\mu - \sigma$  (low),  $\mu$  (medium) and  $\mu + \sigma$  (high). For the dynamic model of the ESS, the sensitivity of each parameter was examined in our previous paper [24]. In this paper, the uncertainty in ESS modeling will focus on its active power availability, i.e., initial SOC ( $\zeta_{ini}$  in Fig. 4). Three testing levels will be implemented for interval optimization:  $\zeta_{ini} = \zeta_{min}$ ,  $\zeta_{ini} = 50\%$  and  $\zeta_{ini} = \zeta_{max}$ , representing low, medium and high conditions respectively. The ability of providing active power support will be limited for both the low and high conditions, where no power output can be made when  $\zeta_{ini} = \zeta_{min}$  and no power input is allowed when  $\zeta_{ini} = \zeta_{max}$ . The total TOAT scenarios tested will then be 9 ( $L_9 4^3$ ), with equal probability for each scenario. Detailed testing scenario setups are shown in Table IV.

TABLE IV  
TOAT TESTING SCENARIOS

Scenario	Variable testing levels ( $l$ )			
	Wind farm 1	Wind farm 2	ESS1 SOC	ESS2 SOC
1	Low	Low	Low	Low
2	Low	Medium	Medium	Medium
3	Low	High	High	High
4	Medium	Low	Medium	High
5	Medium	Medium	High	Low
6	Medium	High	Low	Medium
7	High	Low	High	Medium
8	High	Medium	Low	High
9	High	High	Medium	Low

Furthermore, for simplicity, a linear cost function is assumed for the loads, with its coefficient, i.e., cost of ELS ( $\alpha$ ), set to  $\$10^4/\text{MWh}$  to reflect the significant negative effect on the customers. In practice, nonlinear cost functions can also be directly adapted in the proposed method. The maximum

allowable load shedding percentage is 30% to ensure the continuous supply of electricity to critical loads. The resulting Pareto Frontier that trades off objectives in (10) and (12) and a compromise solution for all credible contingencies are shown in Fig. 5. For comparison purposes, an additional set of simulations were performed, with the only difference being the absence of ESS, i.e., ELS is the only post-contingency corrective control method. Their PFs were also illustrated in Fig. 5. Resulting compromise solutions details, which are annotated in Fig. 5, were calculated with (16) and (17), with the weighting factor of the two objectives set as equal for illustration purpose only.

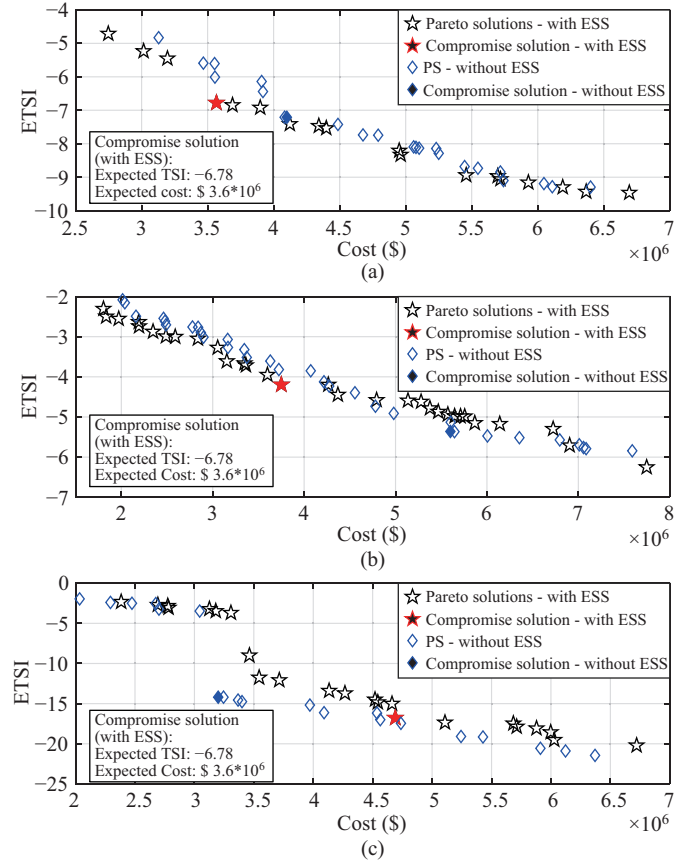


Fig. 5. Pareto Frontiers and Compromise Solutions under 3 contingencies. (a) C1. (b) C2. (c) C3.

For the PFs with both ESS and ELS as EC, which are marked by pentagons in Fig. 5, the method was able to provide 18, 31 and 24 Pareto Solutions for each credible contingency with 50 generations each with 100 individuals.

Broad selection ranges were seen on all three PFs, providing system operators with as many choices as possible. The details of the compromise solution are shown in Table V. Detailed system performance under all considered scenarios are shown in Table VI, with italic fonts marking the scenarios in which systems can self-stabilize without involving EC. It can be seen that the system is stabilized under all scenarios, whether with or without the aid of EC.

The PF for the control methods that only consider ELS are marked by diamonds in Fig. 5, with their compromise

TABLE V  
DETAILS OF COMPROMISE SOLUTION IN FIG. 5

Contingency	ELS Values	ETSI	ECost (\$)	
C1	Area 1	26%	-6.78	$3.6 \times 10^6$
	Area 2	3%		
	Area 3	5%		
	Area 4	2%		
	Area 5	5%		
C2	Area 1	1%	-4.20	$3.8 \times 10^6$
	Area 2	13%		
	Area 3	0%		
	Area 4	19%		
	Area 5	29%		
C3	Area 1	0%	-16.77	$4.7 \times 10^6$
	Area 2	9%		
	Area 3	29%		
	Area 4	20%		
	Area 5	18%		

TABLE VI  
DETAILED SYSTEM PERFORMANCE

Scenario	Contingency		
	C1	C2	C3
1	14.13	7.51	49.11
2	8.57	6.32	48.98
3	10.3	7.86	51.54
4	14.70	7.59	51.19
5	35.88	6.62	50.34
6	29.80	33.86	49.71
7	9.15	5.92	50.55
8	34.02	4.93	51.09
9	26.47	32.66	50.36

solutions described in Table VII. Numerous differences were spotted when comparing PFs that involve ESS in EC with those that do not:

For contingency C1, Pareto Solutions without the consideration of ESS will generally incur higher operational cost under the same ETSI value. When comparing the two compromise solutions, the ELS percentage will be higher in area 5 when no ESSs are involved. This is caused by the vicinity of contingency (fault on bus 4 and tripping line 4–5 after clearance) to the ESS location (bus 8). When no ESSs are considered, increased ELS percentage was seen for area 5 to make up for the effect of ESSs.

For contingency C2, the two PFs were relatively similar, with ESS-less Pareto Solutions dominating the operating cost range between  $\$4.5 \times 10^6$  to  $\$7 \times 10^6$ . Differences in compromise

TABLE VII  
DETAILS OF COMPROMISE SOLUTION WITHOUT ESS

Contingency	ELS Values	ETSI	ECost (\$)	
C1	Area 1	27%	-7.21	$4.1 \times 10^6$
	Area 2	1%		
	Area 3	4%		
	Area 4	5%		
	Area 5	12%		
C2	Area 1	14%	-5.36	$5.6 \times 10^6$
	Area 2	29%		
	Area 3	0%		
	Area 4	12%		
	Area 5	30%		
C3	Area 1	2%	-14.19	$3.2 \times 10^6$
	Area 2	1%		
	Area 3	29%		
	Area 4	14%		
	Area 5	6%		

solutions indicates that though the contingency occurred in area 3, it depended on the increased ELS percentage in area 1 and 2 to stabilize the contingency (fault on bus 21 and tripping line 21–22 after clearance) when ESSs were not considered.

The result output under contingency C3 represented the system performance in which ESSs may not be beneficial in maintaining system security, as the Pareto Solutions when no ESSs were considered led to lower ETSI values with the same operating cost. Similar behavior was also spotted in compromise solution comparison, in which ELS percentage decreases occurred when no ESSs were considered. This indicates that the existing ESSs on bus 8 and 24 may not be ideal in restoring system stability of the post-contingency system topology under contingency C3. Considering the locations of wind farms and ESSs are relatively far from the fault location of C3, the dominant method of control in this situation will be the post-contingency ELS, whose strategy selection will then be less affected by the variation in wind farms and ESSs. Since the control strategy of post-contingency ELS will be identical for every scenario, its optimization will lead to synchronized behavior of improving/deteriorating system stability across all scenarios, which can lead to the sudden increase/decrease of ETSI as seen in Fig. 5(c). This indicates that with flexible operations, the contribution to system stabilization from ESSs may also be limited by its location and rated power.

#### E. Performance Analysis of Energy Storage Systems

To first evaluate the performance of ESS, contingency C1 under scenario 8 was selected as a representative case. According to the results, the system TSI improved from -2.66 (slightly unstable) to 34.02 (stable) with the presence of ESSs. To evaluate the effectiveness of ESS in this case, the performance in terms of both active and reactive power exchange are shown in Fig. 6.

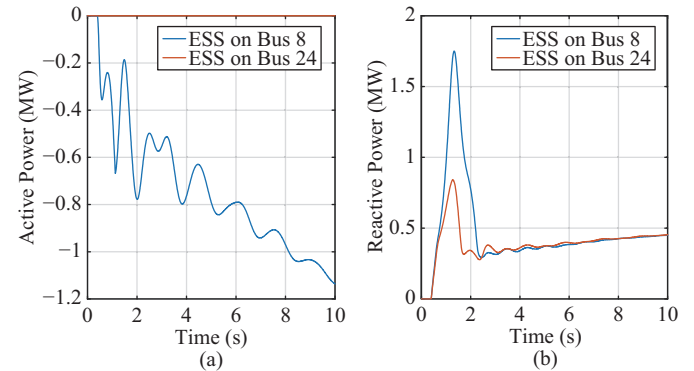


Fig. 6. The power performance of ESS. (a) Active. (b) Reactive.

As wind generation is producing more power than predicted, ESS on bus 8 was required to work in energy storage mode to digest the excess energy in the system. The high SOC condition of ESS on bus 24 constrained its ability to absorb power, but since the ESSs are power electronics-based, they are capable of providing reactive power support regardless of current SOC conditions. This was proved in Fig. 6(b), where ESS on bus 24 was providing a strong support of reactive power to the network. Also, since ESS on bus 8 is located in

the same area as the contingency, it was effective in stabilizing the contingency.

### F. Performance Analysis of Emergency Load Shedding

To illustrate the effect of ELS, two cases will be further investigated: contingency C1 under scenario 6 and contingency C3 under scenario 7. The two cases shared the common characteristics: existing ESSs were not sufficient and relied on ELS to regain system stability. Performance comparisons will focus on two aspects: 1) post-contingency system performance with ESSs installed, which will evaluate both Center-of-Inertia-relative (COI-relative) angles and bus voltage magnitudes, shown in Fig. 7 and Fig. 9; and 2) ESSs, which will compare their active and reactive power support to the system both before and after ELS, shown in Fig. 8 and Fig. 10. Detailed effects of ELS, which effectively alleviates the bus voltages, are illustrated in Fig. 7(d) and Fig. 9(d).

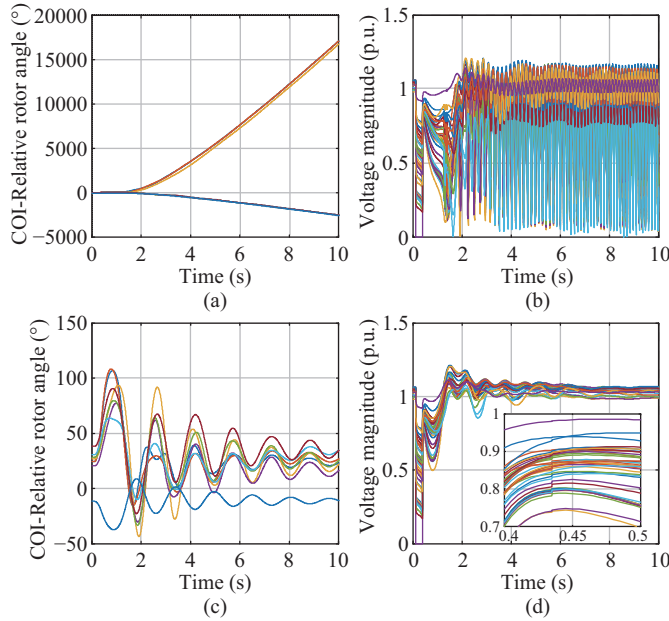


Fig. 7. System response trajectory comparison. (a) COI-relative angle magnitudes prior to ELS. (b) Bus voltage magnitudes prior to ELS. (c) COI-relative angle magnitudes after ELS. (d) Bus voltage magnitudes after ELS.

#### 1) Contingency C1 Scenario 6

In this scenario, more wind power than predicted was generated, with wind generation on bus 30 and 33 being medium and high. The  $\zeta_{ini}$  of ESSs on bus 8 and 24 were low and medium, indicating that both were capable of damping the extra power in the system. The oscillating behavior seen in Fig. 8(a) and (b) indicates that the electric control system of ESSs were actively managing to respond to the unstable system characteristics but made little effect due to their small scales. Moreover, with  $\zeta_{ini} = \zeta_{min}$  for ESS on bus 8, its inability to provide active power support may affect its contribution to regaining system stability. When ELS was applied to the system, the active power absorption required from the ESS on Bus 8 was reduced. Therefore, the ESS on bus 8 was able to function normally and damp the extra power in the system.

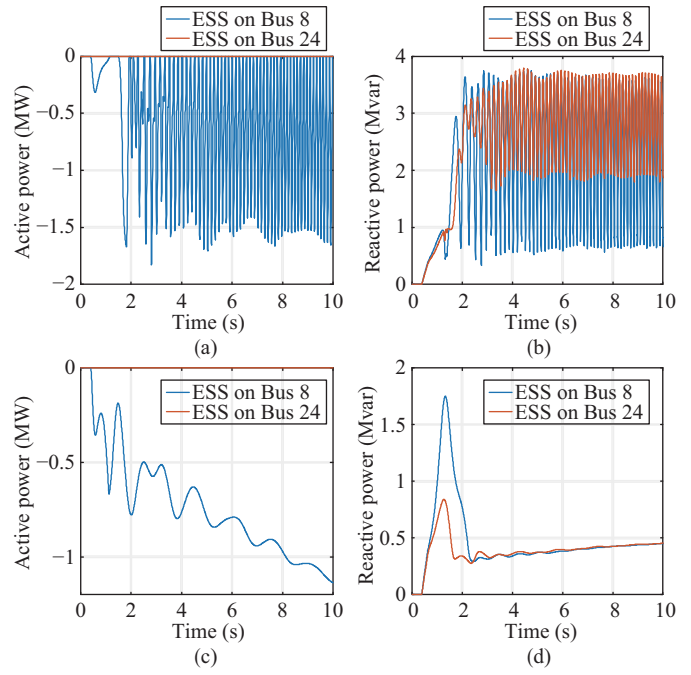


Fig. 8. ESS response trajectory comparison. (a) Active power performance of ESS prior to ELS. (b) Reactive power performance of ESS prior to ELS. (c) Active power performance of ESS after ELS. (d) Reactive power performance of ESS after ELS.

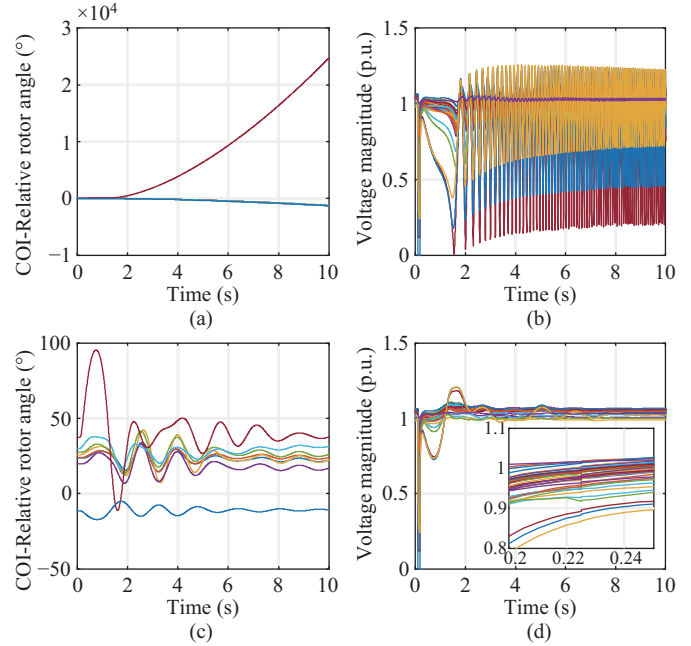


Fig. 9. System response trajectory comparison. (a) COI-relative angle magnitudes prior to ELS. (b) Bus voltage magnitudes prior to ELS. (c) COI-relative angle magnitudes after ELS. (d) Bus voltage magnitudes after ELS.

#### 2) Contingency C3 Scenario 7

In this scenario, wind generation on bus 30 and 33 were high and low, inferring the overall generation approximately matched the load, and only small adjustments were required to improve the system power flow and maintain system stability. This can also be reflected by the behavior of ESSs shown in Fig. 10(a) and (b), where the magnitudes of power exchange

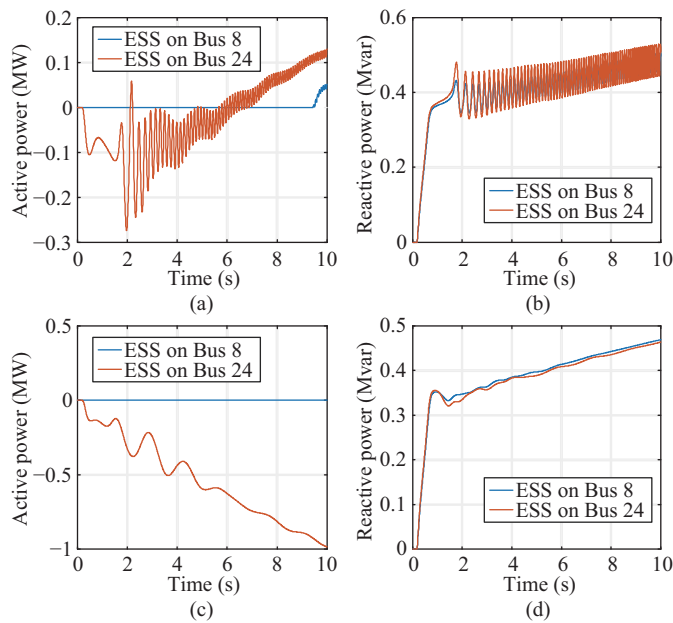


Fig. 10. ESS response trajectory comparison. (a) Active power performance of ESS prior to ELS. (b) Reactive power performance of ESS prior to ELS. (c) Active power performance of ESS after ELS. (d) Reactive power performance of ESS after ELS.

were relatively small. However, flexibility of ESS on bus 8 was limited due to its high  $\zeta_{ini}$  and was unable to absorb power. Similar to the previous case, the electric control module tried and failed to maintain stability by only using ESSs. The execution of ELS reduced the load demand and the ESS on bus 24 then worked in energy absorption mode to accept the extra power generated.

#### G. Performance Analysis of Algorithm

To ensure the fidelity of the system model and the reliability of the solutions, NAA was adopted in this paper to search the optimal solutions in an iterative way. Based on the structure of the proposed method, the computation time is dependent on three aspects: 1) total generation number and population size, 2) total number of contingencies, and 3) total number of scenarios. For the results presented in Section IV-D, 50 generations are considered, each with a population of 100. The total number of contingencies and scenarios are 3 and 9 respectively. The time to calculate stability margin by MATLAB and PSS/E is 0.15 seconds for each individual. Therefore, the total computation time required for each assessment is approximately 5.625 hours. It is also possible to further reduce the time by parallelizing the solution process via parallel computing strategies, such as the method illustrated in [25].

## V. CONCLUSION

It can be argued that the amount of ELS may be over-sufficient to stabilize the system under certain scenarios. However, since the goal of this method is to provide a strategy to stabilize all scenarios under all credible contingencies, it was acceptable to see conservative solutions and have relatively large margins for specific cases.

Uncertainties from integrating renewable energy generators are causing significant consequences in power systems and making it harder to stabilize under the occurrence of severe contingencies. The multi-objective method proposed in this paper provides a novel way to avoid post-contingency system instability by utilizing the flexibility of energy storage systems and the effectiveness of emergency load shedding as emergency control methods. The feasibility of the method was tested on a modified IEEE-39 system. The results prove the effectiveness of the proposed method in providing control strategies for systems with wind uncertainties and limited energy storage system availabilities. By considering multiple significant contingencies, this method was able to provide the system operators with various tradeoff solutions between system performance and operating cost.

## REFERENCES

- [1] Y. Zhang, M. Li, D. Zhao Yang, and K. Meng, "Probabilistic anomaly detection approach for data-driven wind turbine condition monitoring," *CSEE Journal of Power and Energy Systems*, vol. 5, no. 2, pp. 149–158, Jun. 2019.
- [2] P. Kundur, J. Paserba, V. Ajarapu, G. Andersson, A. Bose, C. Canizares, N. Hatziaargyriou, D. Hill, A. Stankovic, C. Taylor, T. Van Cutsem, and V. Vittal, "Definition and classification of power system stability IEEE/CIGRE joint task force on stability terms and definitions," *IEEE Transactions on Power Systems*, vol. 19, no. 3, pp. 1387–1401, Aug. 2004.
- [3] Australian Energy Market Operator (AEMO), Black System South Australia 28 September 2016-Final Report, Available: [http://www.aemo.com.au/-/media/Files/Electricity/NEM/Market\\_Notices\\_and\\_Events/Power\\_System\\_Incident\\_Reports/2017/Integrated-Final-Report-SA-Black-System-28-September-2016.pdf](http://www.aemo.com.au/-/media/Files/Electricity/NEM/Market_Notices_and_Events/Power_System_Incident_Reports/2017/Integrated-Final-Report-SA-Black-System-28-September-2016.pdf)
- [4] X. Xu, H. X. Zhang, C. G. Li, Y. T. Liu, W. Li, and V. Terzija, "Optimization of the event-driven emergency load-shedding considering transient security and stability constraints," *IEEE Transactions on Power Systems*, vol. 32, no. 4, pp. 2581–2592, Jul. 2017.
- [5] Y. Sun, Z. Zhao, M. Yang, D. Jia, W. Pei, and B. Xu, "Overview of energy storage in renewable energy power fluctuation mitigation," *CSEE Journal of Power and Energy Systems*, vol. 6, no. 1, pp. 160–173, Mar. 2020.
- [6] X. J. Li, and S. X. Wang, "A review on energy management, operation control and application methods for grid battery energy storage systems," *CSEE Journal of Power and Energy Systems*, doi: 10.17775/CSEE-JPES.2019.00160.
- [7] U. Datta, A. Kalam, and J. Shi, "Battery energy storage system for transient frequency stability enhancement of a large-scale power system," in *2017 Australasian Universities Power Engineering Conference (AUPEC)*, Melbourne, VIC, Australia, 2017, pp. 1–5.
- [8] A. G. Pillai, P. C. Thomas, K. Sreeranjini, S. Baby, T. Joseph, and S. Sreedharan, "Transient stability analysis of wind integrated power systems with storage using central area controller," in *2013 Annual International Conference on Emerging Research Areas and 2013 International Conference on Microelectronics, Communications and Renewable Energy*, Kanjirapally, India, 2013, pp. 1–5.
- [9] I. Kiaei and S. Lotfifard, "Tube-based model predictive control of energy storage systems for enhancing transient stability of power systems," *IEEE Transactions on Smart Grid*, vol. 9, no. 6, pp. 6438–6447, Nov. 2018.
- [10] F. A. Inthamoussou, J. Pegueroles-Queralt, and F. D. Bianchi, "Control of a supercapacitor energy storage system for microgrid applications," *IEEE Transactions on Energy Conversion*, vol. 28, no. 3, pp. 690–697, Sep. 2013.
- [11] X. K. Xie, Z. Y. Dong, T. J. Zuo, and Y. Xu, "A risk-based stability dispatch of high wind-penetrated power systems with energy storage," in *2018 IEEE Innovative Smart Grid Technologies-Asia (ISGT Asia)*, Singapore, 2018, pp. 1283–1288.
- [12] Á. Ortega and F. Milano, "Generalized model of VSC-based energy storage systems for transient stability analysis," *IEEE Transactions on Power Systems*, vol. 31, no. 5, pp. 3369–3380, Sep. 2016.

- [13] Y. Xue and M. Pavella, "Extended equal-area criterion: an analytical ultra-fast method for transient stability assessment and preventive control of power systems," *International Journal of Electrical Power & Energy Systems*, vol. 11, no. 2, pp. 131–149, Apr. 1989.
- [14] S. W. Xia, X. Luo, K. W. Chan, M. Zhou, and G. Y. Li, "Probabilistic transient stability constrained optimal power flow for power systems with multiple correlated uncertain wind generations," *IEEE Transactions on Sustainable Energy*, vol. 7, no. 3, pp. 1133–1144, Jul. 2016.
- [15] G. S. Peace, *Taguchi Methods: A Hands-On Approach*, Reading, MA: Addison-Wesley, 1993.
- [16] T. Mori, "Mathematical structural of orthogonal arrays," in *Taguchi Methods: Benefits, Impacts, Mathematics, Statistics and Applications*, T. Mori and S. C. Tsai, Eds. New York, NY: ASME, 2011.
- [17] C. A. C. Coello, G. B. Lamont, and D. A. Van Veldhuizen, *Evolutionary Algorithms for Solving Multi-Objective Problems (Genetic and Evolutionary Computation)*. Berlin, Heidelberg: Springer, 2007.
- [18] F. J. Luo, J. H. Zhao, and Z. Y. Dong, "A new metaheuristic algorithm for real-parameter optimization: Natural aggregation algorithm," in *2016 IEEE Congress on Evolutionary Computation (CEC)*, Vancouver, BC, Canada, 2016, pp. 94–103.
- [19] S. Agrawal, B. K. Panigrahi, and M. K. Tiwari, "Multiobjective particle swarm algorithm with fuzzy clustering for electrical power dispatch," *IEEE Transactions on Evolutionary Computation*, vol. 12, no. 5, pp. 529–541, Oct. 2008.
- [20] F. J. Luo, Z. Y. Dong, Y. Y. Chen, and J. H. Zhao, "Natural aggregation algorithm: A new efficient metaheuristic tool for power system optimizations," in *2016 IEEE International Conference on Smart Grid Communications (SmartGridComm)*, Sydney, NSW, Australia, 2016, pp. 186–192.
- [21] Siemens PTI, PSS/E 34 model library, Siemens: New York, NY, USA, 2015.
- [22] Model User Guide for Generic Renewable Energy System Models, Palo Alto, CA: Electric Power Research Institute (EPRI), 2015.
- [23] L. Wu, M. Shahidepour, and Z. Y. Li, "Comparison of scenario-based and interval optimization approaches to stochastic SCUC," *IEEE Transactions on Power Systems*, vol. 27, no. 2, pp. 913–921, May 2012.
- [24] X. K. Xie, Y. C. Zhang, K. Meng, Z. Y. Dong, J. W. Liu, and S. Tang, "Impact of utility-scale energy storage systems on power system transient stability considering operating uncertainties," in *2019 IEEE Innovative Smart Grid Technologies-Asia (ISGT Asia)*, Chengdu, China, 2019.
- [25] K. Meng, Z. Y. Dong, K. P. Wong, Y. Xu, and F. J. Luo, "Speed-up the computing efficiency of power system simulator for engineering-based power system transient stability simulations," *IET Generation, Transmission & Distribution*, vol. 4, no. 5, pp. 652–661, May 2010.



**Xuekuan Xie** (S'15) received the B.Eng. and M.Sc. degrees from the University of Liverpool, Liverpool, UK, and University College London, London, UK, in 2013 and 2014 respectively. He is currently working towards the Ph.D. degree at the University of New South Wales, Sydney, Australia. His research interests include power system modelling, system stability and control, and grid-integration of renewable energy plants and battery energy storage systems.



**Yuchen Zhang** (M'18) received the B.E., B.Com., and Ph.D. degrees from the University of New South Wales, Sydney, Australia, in 2013, 2013, and 2018, respectively. He is currently a research associate at the University of New South Wales, Sydney, Australia. His research interests include power system stability and control, renewable energy systems, smart campus, data analytics and machine learning applications in power engineering.



integration.

**Ke Meng** (M'10–SM'19) received the Ph.D. degree in Electrical Engineering from the University of Queensland, Brisbane, QLD, Australia in 2009. He is currently a Senior Lecturer in the School of Electrical Engineering and Telecommunications, the University of New South Wales, Sydney, NSW, Australia. He was previously a Lecturer with the School of Electrical and Information Engineering, The University of Sydney, Sydney, Australia. His research interests include electric power system modelling, stability analysis, renewable energy systems and grid



**Zhao Yang Dong** (M'99–SM'06–F'17) received the Ph.D. degree in Electrical Engineering from The University of Sydney, Camperdown, NSW, Australia, in 1999. He is currently a SHARP Professor and the Director of UNSW Digital Grid Futures Institute, The University of New South Wales, Sydney, NSW, Australia. He is also the Director of Australian Research Council Research Hub for Integrated Energy Storage Solutions. He was previously a Professor and the Head of School of Electrical and Information Engineering, The University of Sydney, and the Ausgrid Chair and the Director of the Ausgrid Centre for Intelligent Electricity Networks, The University of Newcastle, Australia. He also held industrial positions with Transend Networks (now TAS Networks), Australia. He is a 2019 Highly Cited Researcher, with expertise in smart grid, power system planning, power system security, renewable energy systems, load modeling, electricity market, and computational intelligence and its application in power engineering. He is also an Editor for the *IEEE Transactions on Smart Grid*, *IEEE Power Engineering Letters*, *IET Renewable Power Generation*, and *IET Smart City*.



**Junwei Liu** (S'15–M'18) received the B.E. degree in Electrical Engineering (Power) from the University of Sydney, Australia, in 2015 and the Ph.D. degree in Electrical Engineering at the University of New South Wales, Australia in 2018. His research interests include power system planning, voltage stability and control, FACTS devices planning and control, reactive power planning and enhancement, dynamic load modelling, optimization algorithm development, and renewable energy penetration.